GU J Sci, Part C, 10(4): 1059-1069 (2022)

Gazi University

Journal of Science

PART C: DESIGN AND TECHNOLOGY

http://dergipark.gov.tr/gujsc

Photoresponse of the Al/n-Si Schottky Diode with Nanorod ZnO Interface Layer Prepared Using Hydrothermal Method

Neslihan TURAN , orcid no: 0000-0001-8933-2762

Gazi University, Faculty of Science, Department of Physics, 06500, Yenimahalle/Ankara/TÜRKİYE

Article Info

Research article
Received: 7.10.2022
Revision: 1.11.2022
Accepted: 9.11.2022

Keywords

Hydrothermal
Zinc oxide
Photovoltaic
nanorod

Abstract

In this study, ZnO nanorods (ZnO-NR) were prepared on n-Si wafer by hydrothermal method. Structural and morphologic properties of ZnO nanostructures were investigated through XRD and SEM method. The illumination impacts on the current-voltage (I-V) measurements of the prepared Al/ZnO-NR/n-Si diode were explored in the dark and different illumination intensities (20–100 mW/cm^2) between ± 1.5 V bias voltage range. The Schottky diode barrier height value had an increasing trend with increasing illumination intensity from 20 to 100 mW/cm^2 while the ideality factor had a decreasing trend with the increase of photocurrent. The temporary photocurrent increases as illumination intensity increases. The slope (α) of the logI_{ph}-log$P$ curve was obtained as 0.618 and this slope confirmed that this ZnO nanorod shows photoconducting behavior. The short-circuit current (I_{sc}) and open-circuit voltage (V_{oc}) values were obtained to be 774.08 µA and 0.24 V under 100 mW/cm^2 illumination intensity, respectively. The prepared Al/ZnO-NR/n-Si diode showed both photodiode and photovoltaic properties under different light intensities. It was concluded that the prepared Al/ZnO-NR/n-Si diode can be used in the optoelectronic applications, especially for the photodiode industry.

1. INTRODUCTION

In metal-semiconductor (MS) structures, the interfacial layer between the MS structure will affect many parameters of the diode, and changes in the thickness and concentration of the interface material affect the electrical behavior of the structure. The study of changes in the properties of MS structures using many materials as interfaces still attracts great interest. By using different production techniques and various materials, doped or layered structures are obtained and the changes in the electrical properties of these structures are examined. ZnO is a well-known semiconductor and functional material used in many places such as chemical sensors, conductivity electrodes, photoelectric devices, and solar cells, etc. The development of photovoltaic technology is to increase the efficiency of cells and reduce the cost of production, making them more suitable for various applications.

It can be produced by many methods such as physical [1–4] (ball milling, chemical and physical vapor deposition, lithographic, laser ablation, etc.), chemical (solution-oriented synthesis, gas phase reaction) and biological methods, and the properties of nanostructures change according to the production methods. Compared to other methods, solution-oriented methods show advantages such as low production cost, scalability, ease of application, and relatively low temperatures (<200 °C) are required for production. Due to these advantages, solution-oriented methods attract attention and ZnO can be produced by hydrothermal/solvothermal [5–7], precipitation, sol-gel [8], chemical bath deposition [9, 10], and electrochemical deposition [11]. Because there are too many effects in solution-oriented methods, the nanoscale effects are different, and ZnO can be produced in different structures such as nanorods [12], nanoflowers [13, 14], nanoarrays [15, 16], and nanospheres [17, 18]. The electrical conductivity and optical properties of ZnO change with the change of their morphological structure. ZnO nanorod structures attract research attention due to their large surface area, low cost and ease of use in potential applications in optoelectronic fields. ZnO nanorods can be produced effectively using the hydrothermal method [19]. ZnO

e-mail: neslihanturan@gazi.edu.tr
DOI: 10.29109/gujsc.1185766

nanowires/nanorods are used in various nanodevice applications such as solar cells [20], nanogenerator [21], field emitters [22], gas sensors [23], and UV detectors [24].

In this article, the Al/ZnO-NR/n-Si/Al device was prepared using the hydrothermal method, and it was investigated whether it is practical for photovoltaic devices with I-V measurements in the range of ± 1.5 V in the dark and various illumination intensities.

2. MATERIALS AND METHODS

In this study, ZnO-NR were synthesized on n-Si wafer by hydrothermal method. Before the growth of ZnO-NR, a thin ZnO seed layer was coated on the surface of n-Si wafer. First n-type Si wafer (orientation *100*, thickness 525 μm, and resisivity 1-20 Ω·cm) was cleaned with an ultrasonic cleaner using cleaning steps with chloroform, acetone, and methanol. The oxide structure was removed using a mixture of HF-deionized water (1:10), rinsed with deionized water, and dried. Aluminum (99.99% purity) was evaporated as a ohmic contact on the back of the wafer under 10^{-6} Torr vacuum using the thermal evaporation system.

Secondly, the seed layer was prepared by spin coating technique using zinc acetate dihydrate ($Zn(CH_3COO)2•2H_2O$), methanol, and NaOH precursors. Zinc acetate dihydrate was dissolved in 100 ml methanol on the magnetic stirrer. Then, NaOH (33%) was dropped slowly to the 0.02 M zinc acetate dihydrate solution. The solution was stirred at 60°C for 2 h on magnetic stirrer. The resultant transparent solution was cooled room temperature and was dropped on n-Si wafer. 500 rpm for 5 s and 3000 rpm for 30 s were chosen as the spin coating parameters. After the coating, the substrate was annealed at 130°C for 5 min in oven and this coating procedure was repeated four times.

For the hydrothermal process, ZnO was prepared using Zinc acetate dihydrate, deionized water, and ammonia (25%). Zinc acetate dissolved in deionized water (0.05 M), then 1.5 ml ammonia dropped slowly in the solution on magnetic stirrer. Wafer inserted into teflon container with the seed layer side down, and the solution was added to hydrothermal system which was set to 90 °C for 12 h. After the system cooled down to room temperature naturally, wafer was taken out of the hydrothermal system, rinsed with deionized water, and dried. Finally, For the Al/ZnO-NR/n-Si/Al structure, the top contact was obtained by deposition of Al with a thickness of 150 nm and a diameter of 2.75 mm, under 10^{-6} torr pressure, with a thermal evaporation system. Schmetic representation of experimental procedure is shown in Fig. 1.

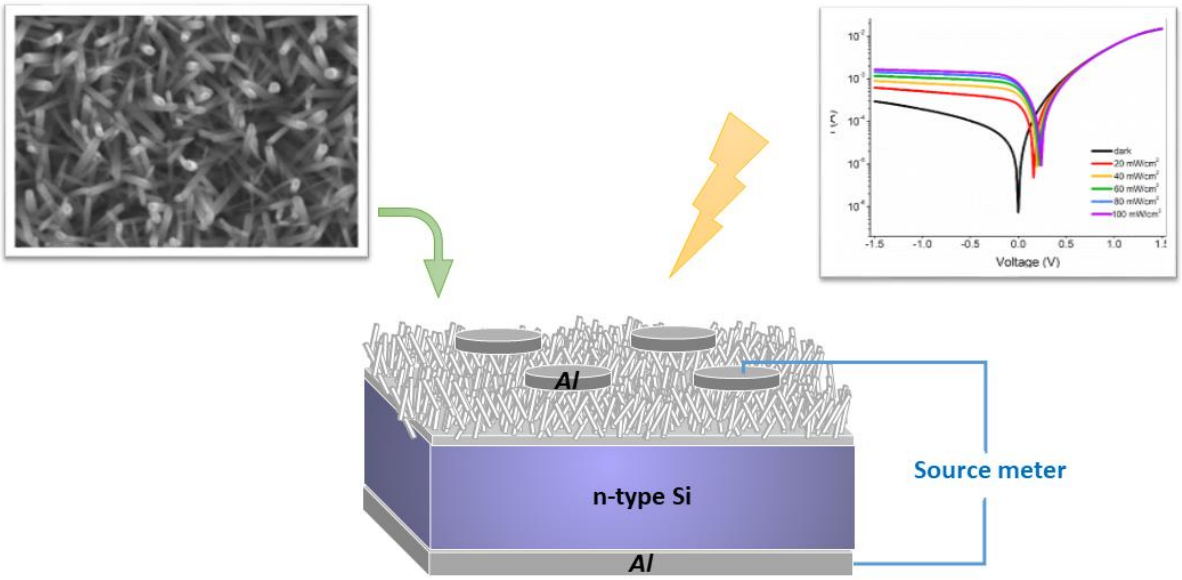

Fig. 1. *Schematic representation of experimental procedure*

The crystallographic and morphologic properties of ZnO-NR were characterized by Bruker D8 Advance diffractometer and FE-SEM (Hitachi SU5000) respectively. The (I-V) measurements of the Al/ZnO-NR/n-Si/Al in ± 1.5 V bias voltage range was performed under the dark and various illumination intensities using the FYTRONIX solar simulator and Keithley 2400 at room temperature.

3. RESULTS

The surface morphology of the sample identified by FE-SEM is shown in Fig 2. a and b are the surface views above, and c is the cross-section view. It was observed that nanorods were formed on the surface and their orientation was random in the c direction. When the c-oriented nanorods in Figure 2b were examined, it was seen that the ZnO nanorods had a hexagonal structure. The thickness of the ZnO nanorod layer on the surface is approximately 350–400 nm, as can be seen in the cross-sectional view in Figure 2c.

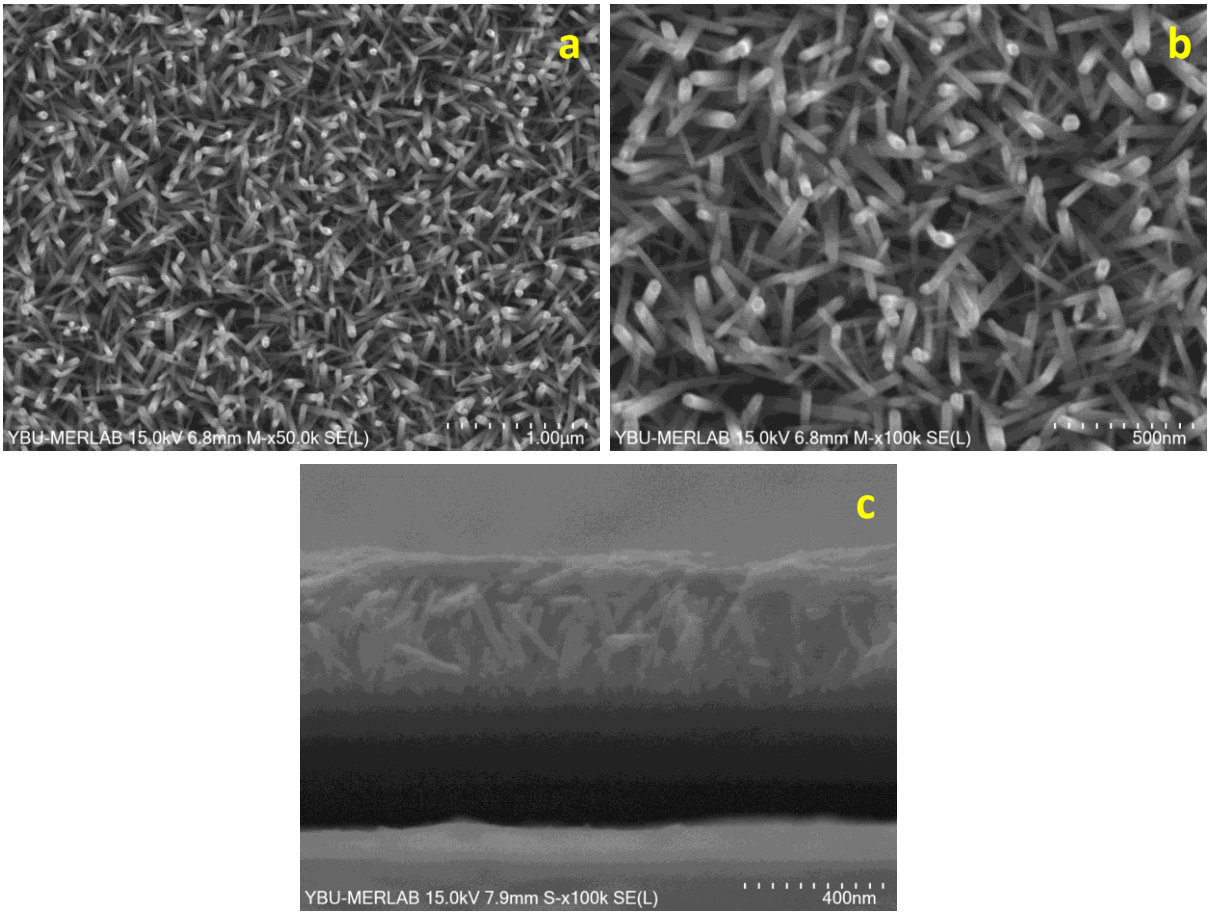

Fig. 2. *SEM images of the Al/ZnO-NR/n-Si structure a) X50k b) X100k c) cross-section view*

Fig. 3 shows the XRD pattern of ZnO-NR grown on n-Si recorded in the range of 2θ=10–80°. The diffraction peak of the (002) of ZnO-NR was marked in the diffraction pattern. The peak is compatible with the JCPDS 36–1451 pdf card belonging to ZnO hexagonal wurtzite (space group $P6_3mc$). The peak belonging to the n-Si in the XRD diffraction pattern were also observed.

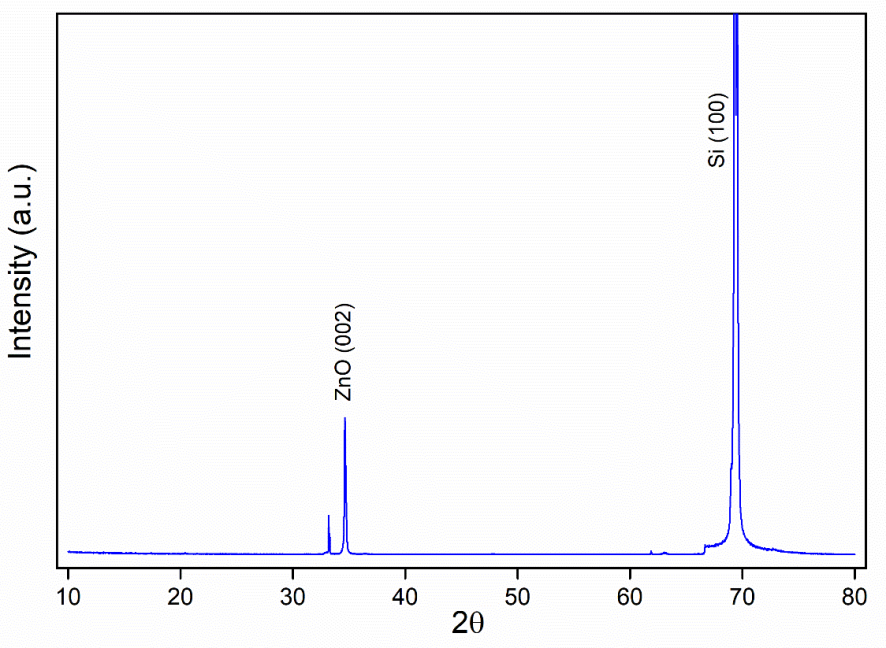

Fig. 3. *XRD pattern of the Al/ ZnO-NR/n-Si structure*

The current-voltage (*I–V*) measurements of the fabricated Al/ZnO-NR/n-Si Schottky diode according to thermionic emission (TE) theory were investigated from in dark and various illumination intensities. The current-voltage equation in reverse and forward bias can be defined by the following relation [25–29]

$$I = I_0 exp\left(\frac{qV}{nkT}\right)\left[1 - exp\left(-\frac{qV}{kT}\right)\right] \quad (1)$$

Where

$$I_0 = AA^*T^2 exp\left[-\frac{q\Phi_B}{kT}\right] \quad (2)$$

where Φ_B is the Schottky barrier height, k is the Boltzmann constant, q is the charge of electron, T is the absolute temperature, n is the ideality factor, A^* is the effective Richardson constant of 112 $Acm^{-2}K^{-2}$ for n-Si, A is the area of effective diode and I_0 is the saturation current of reverse. From the forward bias $lnI-V$ measurement by using Eq. 1 and Eq. 2, the barrier height and ideality factor of the fabricated sample can be estimated using the Eq. 3 and Eq. 4 [30–32]

$$n = \frac{q}{kT}\frac{dV}{d(lnI)} \quad (3)$$

$$\Phi_B = \frac{kT}{q} ln\left(\frac{AA^*T^2}{I_0}\right) \quad (4)$$

The logarithmic current-voltage (*I-V*) measurements of the ZnO-NR film deposited in Al/n-Si interface, including the illustration of the between ±1.5 V and in the illumination intensity range of 20–100 mW/cm^2 and in dark are indicated in Fig 4.

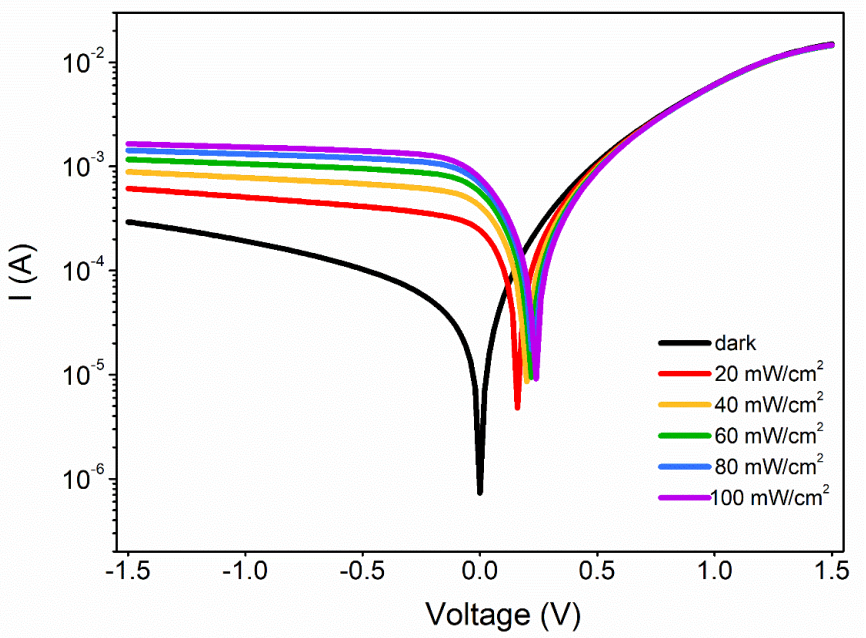

Fig. 4. *Current-voltage characteristics of* Al/ZnO-NR/n-Si *dark and under various illumination intensities*

As can be seen from the forward bias part of Fig. 4, the *I-V* curve shifts toward the positive voltage as the illumination intensity increases. This situation corresponds to photovoltaic behavior. The dark characteristics of the produced Al/ZnO-NR/n-Si diode showed good rectification behavior. While the ratios of the forward current and reverse current in the dark and 100mW/cm^2 intensity are 50.9 and 8.9 at 1.5 V, respectively. As can be seen from the different illumination characteristics in Fig. 4, the produced diode showed both photodiode properties in reverse bias and photovoltaic properties in forward bias. Using Eq. 3 and Eq. 4, n, Φ_B , and I_0 values were calculated in the dark and at various illumination intensities and are given in Table 1.

Table. 1. *Variation of electrical parameters with various illumination intensity of Al/ZnO-NR/n-Si Schottky diode*

Illumination intensity (mW/cm^2)	n	Φ_B (eV)	I_0 (μA)	I_{ph} (μA)	R_s (Ω)	R_{sh} (Ω)	V_{oc} (V)	I_{sc} (μA)
0	2.92	0.631	15.40	------	84.4	5955	------	------
20	2.49	0.672	3.13	613	89.5	5462	0.16	244
40	2.28	0.693	1.38	887	91.2	5206	0.20	417
60	2.05	0.713	0.64	1161	92.8	5003	0.22	566
80	1.97	0.728	0.37	1423	93.5	4844	0.22	685
100	1.66	0.758	0.11	1646	94.4	4628	0.24	774

The fourth region data of the *I–V* measurements are shown in Fig. 5. The open circuit voltage (V_{oc}) and short circuit current (I_{sc}) values are determined from the points where the curves of *I–V* intersect the voltage and current axis, respectively. As observed in Fig. 5 and Table 1, the I_{sc} and V_{oc} values increase as illumination intensity increases. For example, the values of I_{sc} and V_{oc} are found 244 μA and 0.16 V for 20 mW/cm^2 and 774 μA and 0.24 V for 100 mW/cm^2, respectively. This depicts that the Au/ZnO-NR/n-Si Schottky diode is completely sensitive to illumination intensity and shows photovoltaic behavior.

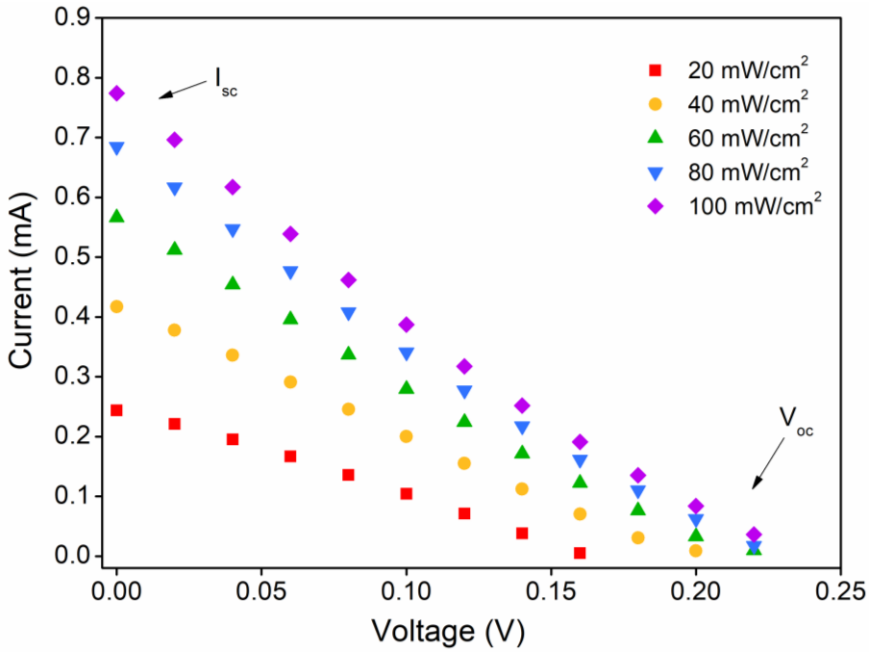

Fig. 5. *I–V plots for the Al/ZnO-NR/n-Si Schottky diode*

As the illumination intensity increases, the n and I_0 values decrease, while the Φ_B value increases. For example, The n values decreased from 2.92 in the dark to 1.66 at 100 mW/cm^2 and the Φ_B values increased from 0.631 eV in the dark to 0.758 eV at 100 mW/cm^2. It was determined from Fig. 4 that the diode produced due to the photocurrents (I_{ph}) increasing in reverse bias as illumination intensity increases was a photodiode. I_{ph} values for 20 mW/cm^2 and 100 mW/cm^2 were found as 613 μA and 1646 μA, respectively.

Both the series resistance (R_s) in the forward bias and the shunt resistance (R_{sh}) in the reverse bias affect the electrical properties of the produced diode. R_s and R_{sh} values were found by Ohm's law ($R_i = dV/dI$) and are illustrated in Table 1 and Fig. 6.

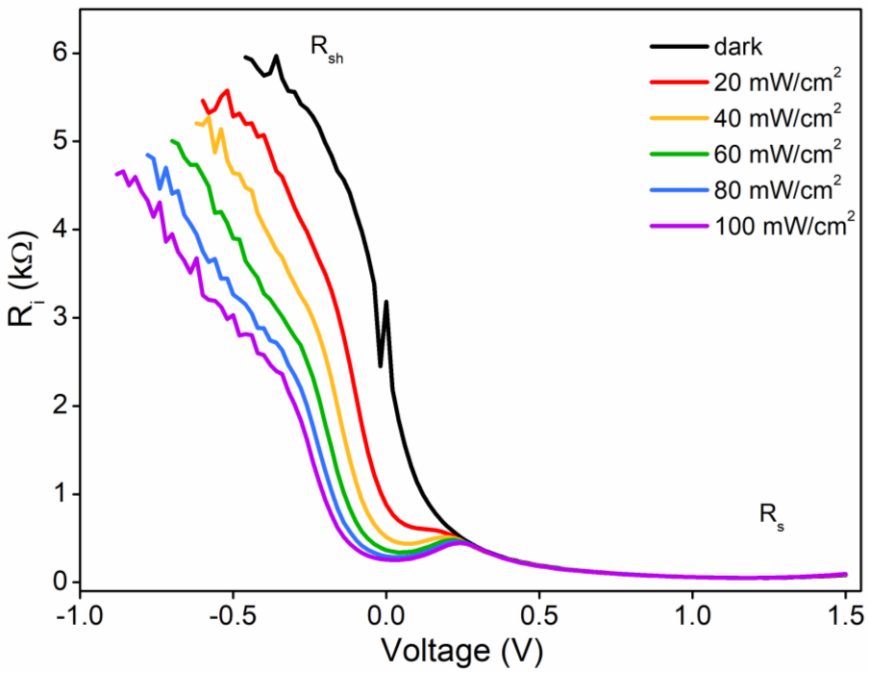

Fig. 6*. The* R_i*-V plots at dark and under various illumination intensities*

While R_s values almost do not change under illumination, R_{sh} values decrease with increasing illumination intensity. Hence, R_s values in dark and 100 mW/cm^2 were found as 84 Ω and 94 Ω at 1.5V for the produced diode, respectively. R_{sh} values in dark and 100 mW/cm^2 were found as 5748 Ω and 2578 Ω at -0.4V for the produced diode, respectively.

In addition to the *I-V* measurements, current-time (*I-t*) measurements were performed under different illumination intensities to investigate the photosensitivity of the produced diode at -1V and are illustrated in Fig 7. From Fig. 7, it has been observed that the current increases when the light is on and decreases when the light is off. That is, the photocurrent for Al/ ZnO-NR /n-Si diode was observed when the light was on. This photocurrent increased as the light intensity increased from 20 to 100 mW/cm^2. This behavior is due to charge trapping at deep levels [33].

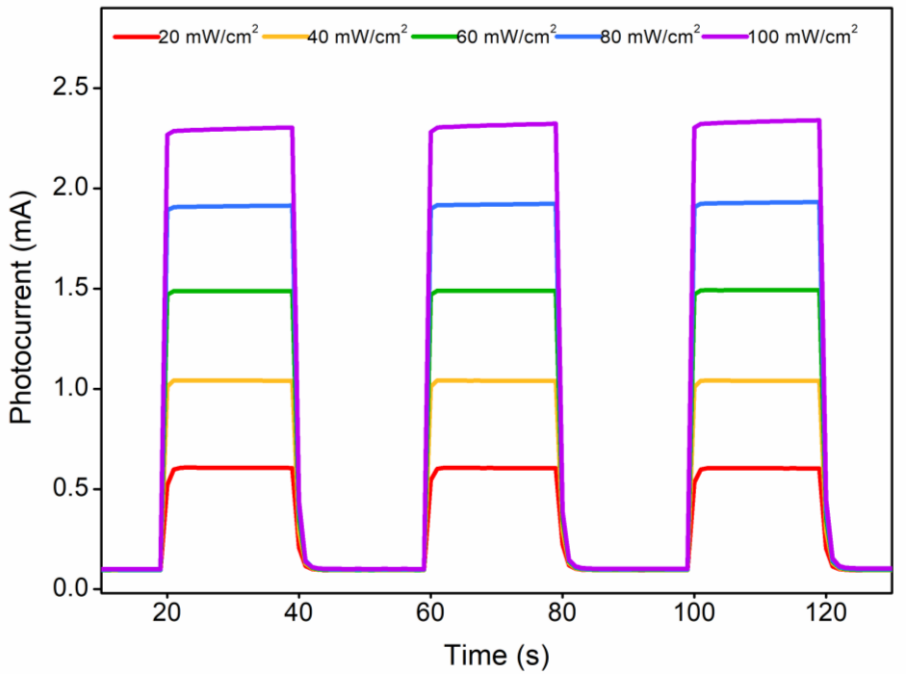

Fig. 7. *Transient photocurrent characteristics of Al/ZnO-NR/n-Si at various illumination intensity.*

To determine the variation of the photoconduction via the various illumination intensity, the double-logarithmic photocurrent (I_{ph}) versus illumination intensity (P) at -1.5V was plotted and shown in Fig. 8. The mechanism of photoconduction can be found by the Eq. 5 [34].

$$I_{ph} = P^{\alpha} \tag{5}$$

Where, α, I_{ph}, and A are a power exponent, the photocurrent, and a constant, respectively.

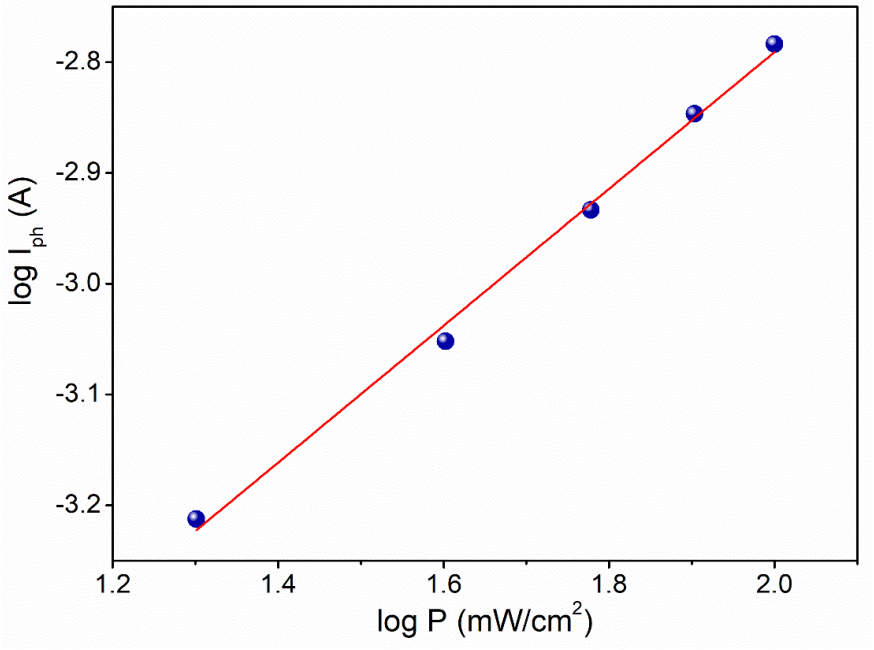

Fig. 8. *log (I_{ph}) vs log (P) plot for the Al/ZnO-NR/n-Si*

The α value was found from the slope of the logI_{ph}-log$P$ curve and obtained as 0.618 The linear variation of the photocurrent from Fig. 8 is due to trapping of charge carriers at deep levels [35]

4.CONCLUSIONS

ZnO nanorods were successfully produced on n-Si by hydrothermal method. It has been observed by SEM images that the diameter of the hexagonal ZnO nanorods is around 60 nm and the thickness on the surface is approximately 350–400 nm. In XRD analysis, the characteristic 002 peak of the hexagonal wurtzite structure of ZnO nanorods was observed. The reverse and forward bias current-voltage (*I-V*) characteristics of the prepared Al/ZnO-NR/n-Si photodiode have been analyzed under dark, 20, 40, 60, 80, and 100 mW/cm^2 illumination intensity at room temperature. The main electrical parameters such as,n Φ_B,I_0,I_{ph}, R_s, R_{sh},V_{oc}, and I_{sc} of the fabricated Schottky barrier diode were investigated. It was observed that as the illumination intensity increased, the n values decreased and the Φ_B values increased. The results showed that the electrical parameters are sensitive to illumination intensity and the Al/ZnO-NR/n-Si Schottky barrier diode has photovoltaic and photodiode properties. It is concluded that the produced diode can be used as a photodiode in optoelectronic applications.

REFERENCES

1. Hamid N, Suhaimi S, Othman MZ, Ismail WZW (2021) A Review on Thermal Evaporation Method to Synthesis Zinc Oxide as Photocatalytic Material. Nano Hybrids Compos 31:55–63. https://doi.org/10.4028/www.scientific.net/NHC.31.55

2. Skowronski L, Ciesielski A, Olszewska A, et al (2020) Microstructure and optical properties of E-beam evaporated zinc oxide films-effects of decomposition and surface desorption. Materials (Basel) 13:1–17. https://doi.org/10.3390/MA13163510

3. Müller R, Gelme O, Scholz JP, et al (2020) Epitaxial ZnO layer growth on Si(111) substrates with an intermediate AlN nucleation layer by methane-based chemical vapor deposition. Cryst Growth Des 20:6170–6185. https://doi.org/10.1021/acs.cgd.0c00907

4. Naveed A, Haq U, Nadhman A, et al (2017) Synthesis Approaches of Zinc Oxide Nanoparticles:

The Dilemma of Ecotoxicity. https://doi.org/10.1155/2017/8510342

5. Cheng K, Cheng G, Wang S, et al (2007) Surface states dominative Au Schottky contact on vertical aligned ZnO nanorod arrays synthesized by low-temperature growth. New J Phys 9:. https://doi.org/10.1088/1367-2630/9/7/214

6. Yi F, Huang Y, Zhang Z, et al (2013) Photoluminescence and highly selective photoresponse of ZnO nanorod arrays. Opt Mater (Amst) 35:1532–1537. https://doi.org/10.1016/j.optmat.2013.03.018

7. Shao Z, Li X (2016) Direct-current piezoelectric nanogenerator based on p-Si/n-ZnO heterojunction. Phys E Low-Dimensional Syst Nanostructures 77:44–47. https://doi.org/10.1016/j.physe.2015.11.003

8. Sheikhi S, Aliannezhadi M, Shariatmadar Tehrani F (2022) Effect of precursor material, pH, and aging on ZnO nanoparticles synthesized by one-step sol–gel method for photodynamic and photocatalytic applications. Eur Phys J Plus 137:. https://doi.org/10.1140/epjp/s13360-021-02252-8

9. Maria G, Mari D, Mineo G, et al (2022) Low-Cost , High-Yield ZnO Nanostars Synthesis for Pseudocapacitor Applications. 1–13

10. Azmi ZH, Mohd Aris SN, Abubakar S, et al (2022) Effect of Seed Layer on the Growth of Zinc Oxide Nanowires by Chemical Bath Deposition Method. Coatings 12:. https://doi.org/10.3390/coatings12040474

11. Serrà A, Zhang Y, Sepúlveda B, et al (2019) Highly active ZnO-based biomimetic fern-like microleaves for photocatalytic water decontamination using sunlight. Appl Catal B Environ 248:129–146. https://doi.org/10.1016/j.apcatb.2019.02.017

12. Hajijamali Z, Khayatian A, Almasi Kashi M (2020) Etching of ZnO nanorods by ZnO nanoparticles and adjustment of morphological and UV photodetection properties. J Sol-Gel Sci Technol 95:109–118. https://doi.org/10.1007/s10971-020-05287-y

13. Liao F, Han X, Zhang Y, et al (2017) Hydrothermal synthesis of flower-like zinc oxide microstructures with large specific surface area. J Mater Sci Mater Electron 28:16855–16860. https://doi.org/10.1007/s10854-017-7602-2

14. Wang Y, Li X, Wang N, et al (2008) Controllable synthesis of ZnO nanoflowers and their morphology-dependent photocatalytic activities. Sep Purif Technol 62:727–732. https://doi.org/10.1016/j.seppur.2008.03.035

15. Rivera VF, Auras F, Motto P, et al (2013) Length-dependent charge generation from vertical arrays of high-aspect-ratio ZnO nanowires. Chem - A Eur J 19:14665–14674. https://doi.org/10.1002/chem.201204429

16. Kwon J, Hong S, Lee H, et al (2013) Direct selective growth of ZnO nanowire arrays from inkjet-printed zinc acetate precursor on a heated substrate. Nanoscale Res Lett 8:1–6. https://doi.org/10.1186/1556-276X-8-489

17. Saleh SM (2019) ZnO nanospheres based simple hydrothermal route for photocatalytic degradation of azo dye. Spectrochim Acta - Part A Mol Biomol Spectrosc 211:141–147. https://doi.org/10.1016/j.saa.2018.11.065

18. Bakrudeen HB, Tsibouklis J, Reddy BSR (2013) Facile fabrication of mesoporous ZnO nanospheres for the controlled delivery of captopril. J Nanoparticle Res 15:. https://doi.org/10.1007/s11051-013-1505-9

19. Zhang Y, Ram MK, Stefanakos EK, Goswami DY (2012) Synthesis, characterization, and applications of ZnO nanowires. J Nanomater 2012:. https://doi.org/10.1155/2012/624520

20. Wibowo A, Marsudi MA, Amal MI, et al (2020) ZnO nanostructured materials for emerging solar cell applications. RSC Adv 10:42838–42859. https://doi.org/10.1039/d0ra07689a

21. Le AT, Ahmadipour M, Pung SY (2020) A review on ZnO-based piezoelectric nanogenerators: Synthesis, characterization techniques, performance enhancement and applications. J Alloys Compd 844:156172. https://doi.org/10.1016/j.jallcom.2020.156172

22. Chen HW, Yang HW, He HM, Lee YM (2015) ZnO nanorod arrays prepared by chemical bath deposition combined with rapid thermal annealing: Structural, photoluminescence and field emission characteristics. J Phys D Appl Phys 49:. https://doi.org/10.1088/0022-3727/49/2/025306

23. Jagadale SB, Patil VL, Vanalakar SA, et al (2018) Preparation, characterization of 1D ZnO nanorods and their gas sensing properties. Ceram Int 44:3333–3340. https://doi.org/10.1016/j.ceramint.2017.11.116

24. Kwon DK, Porte Y, Ko KY, et al (2018) High-Performance Flexible ZnO Nanorod UV/Gas Dual Sensors Using Ag Nanoparticle Templates. ACS Appl Mater Interfaces 10:31505–31514. https://doi.org/10.1021/acsami.8b13046

25. Rhoderick EH, Williams RH (1988) Metal-Semiconductor Contacts. Clarendon Press, Oxford

26. Iwai H, Sze SM, Taur Y, Wong H (2013) MOSFETs. Wiley, New York

27. Kaplan N, Taşcı E, Emrullahoğlu M, et al (2021) Analysis of illumination dependent electrical characteristics of α- styryl substituted BODIPY dye-based hybrid heterojunction. J Mater Sci Mater Electron 16738–16747. https://doi.org/10.1007/s10854-021-06231-8

28. Şahin MF, Taşcı E, Emrullahoğlu M, et al (2021) Electrical, photodiode, and DFT studies of newly synthesized π-conjugated BODIPY dye-based Au/BOD-Dim/n-Si device. Phys B Condens Matter 614:. https://doi.org/10.1016/j.physb.2021.413029

29. Tezcan AO, Eymur S, Taşcı E, et al (2021) Investigation of electrical and photovoltaic properties of Au/n-Si Schottky diode with BOD-Z-EN interlayer. J Mater Sci Mater Electron 32:12513–12520. https://doi.org/10.1007/s10854-021-05886-7

30. Turut A, Karabulut A, Ejderha K, Biyikli N (2015) Capacitance-conductance-current-voltage characteristics of atomic layer deposited Au/Ti/Al2O3/n-GaAs MIS structures. Mater Sci Semicond Process 39:400–407. https://doi.org/10.1016/j.mssp.2015.05.025

31. Tuğluoğlu N, Koralay H, Akgül KB, Çavdar (2016) Analysis of inhomogeneous device parameters using current–voltage characteristics of identically prepared lateral Schottky structures. Indian J Phys 90:43–48. https://doi.org/10.1007/s12648-015-0722-8

32. İlhan M, Koç MM, Coşkun B, et al (2021) Cd dopant effect on structural and optoelectronic properties of TiO2 solar detectors. J Mater Sci Mater Electron 32:2346–2365. https://doi.org/10.1007/s10854-020-05000-3

33. Özcan E, Topaloğlu Aksoy B, Tanriverdi Eçik E, et al (2020) Fabrication of hybrid photodiode systems: BODIPY decorated cyclotriphosphazene covalently grafted graphene oxides. Inorg Chem Front 7:2920–2931. https://doi.org/10.1039/d0qi00468e

34. Bouricha B, Souissi R, Bouguila N, et al (2019) Positive and negative photoconductivity in sprayed β-In2S3 thin films. Mater Res Express 6:116456. https://doi.org/10.1088/2053-1591/ab51c7

35. Yakuphanoglu F, Aslam Farooq W (2011) Photoresponse and electrical characterization of photodiode based nanofibers ZnO and Si. Mater Sci Semicond Process 14:207–211. https://doi.org/10.1016/j.mssp.2011.02.017